Signature quasinormal modes of Ellis-Bronnikov wormhole embedded in warped braneworld background

Antariksha Mitra* and Suman Ghosh†

Department of Physics, Birla Institute of Technology, Ranchi 835215, India

(Received 29 December 2023; accepted 9 February 2024; published 4 March 2024)

We examine the quasinormal modes of Ellis-Bronnikov wormholes embedded in a warped five-dimensional braneworld background and compare with its four-dimensional counterpart. These scalar quasinormal frequencies are obtained using the WKB formula, Prony method, and the direct integration method. The signature of the warped extra dimension shows up as two distinct quasinormal ringing eras, characterized by two distinct dominant quasinormal modes. Features of the latter region are similar to that observed earlier for massive scalar fields in the black hole background, particularly the existence of arbitrarily long-lived quasinormal modes. We also discuss the how steepness of the neck of the wormhole effects the quasinormal frequencies.

DOI: 10.1103/PhysRevD.109.064005

I. INTRODUCTION

Wormholes are known to be solutions of Einstein field equations, like the Schwarzschild black hole in vacuum, that essentially connects two distinct spacetime points within our Universe (intra-universe) or two "parallel universes" (inter-universe) creating a shortcut that allows "apparently faster than light" travel. Detailed historical accounts of theoretical discovery/construction of wormholes could be found, for example, in [1,2]. The original wormhole solutions were found to be nontraversable [3–6] or unstable under perturbation. Violation of the (averaged) null energy condition is required to prevent the wormhole "throat" from collapsing and making it traversable. This could be realized by introducing exotic matter around the throat [7,8]. It appears as if such matters may have a quantum origin, but the standard model matter seems to be inadequate for the generation of macroscopic wormholes [9]. Remarkably, a plethora of wormhole constructions under the so-called modified theories of gravity exist in the literature that avoid the use of exotic matter [10–26]. It has also been suggested that violation can be restricted to arbitrarily small regions [27].

The four-dimensional Ellis-Bronnikov (4D-EB) spacetime [28,29] that employs a phantom scalar field (a field with negative kinetic term) is one of the most researched wormhole geometries since its introduction in 1973. Several studies on this class of model can be found in the literature, including geometry of spinning 4D-EB spacetime [30], generalized spinning of a 4D-EB wormhole in scalar-tensor theory [31], hairy Ellis wormhole solutions [32], Ellis wormholes in anti–de Sitter space [33], and stability analysis of 4D-EB solution in higher-dimensional spacetime [34]. Kar *et al.* presented a generalized version of 4D-EB (4D-GEB) spacetime [35], where the need for exotic matter is *partially* evaded by introducing a new wormhole parameter, $n \geq 2$ ($n = 2$ corresponds to 4D-EB geometry). Quasinormal modes (QNMs), echoes, and some other aspects of 4D-GEB wormholes are analyzed in [36].

Wormholes are yet contemplated as conjectural. However, recent developments in black hole observation [37] have increased the possibility to distinguish a black hole from a so-called black hole mimicker such as a wormhole. In fact, we are far from identifying a black hole from what we have observed yet [38]. In principle, one may identify wormholes through lensing effects, shadows, Einstein rings, and other phenomena [39–45], which may in turn favor modified gravity theories over general relativity. QNMs [46–53] are one such signature that characterizes, e.g., the late time response ("ringing") of a black hole (or wormhole) under perturbation. Dominant quasinormal frequencies (QNFs) can be seen in the gravitational wave signals from black holes (or similar compact objects) at late times. They have been observed recently by LIGO/VIRGO Collaborations [54–57]. Remarkably, observation of a multimode quasinormal spectrum has been reported in [58]. This allows one to determine the individual black hole/wormhole parameters involved. Determination of QNFs with high accuracy is an important challenge and can constrain various modified gravitational theories and also test the strong gravity regime.

One class of the modified theories of gravity involves extra spatial dimension(s). In fundamental physics, the emergence of an additional spatial dimension is

*antarikshamitra@prl.res.in
†suman.ghosh@bitmesra.ac.in

ubiquitous—Kaluza and Klein [59,60] first demonstrated it in an effort to combine gravity and electromagnetic theories for a five-dimensional (5D) gravity model in 1921 and 1926, respectively. Be it the string theory [61] or in the context of symmetries of particle physics (the octonionic hypotheses) [62–67], the extra dimensions seem to appear *naturally*. String theory also motivated the braneworld scenarios—where our four-dimensional Universe (3-brane) is embedded in a higher-dimensional bulk. The so-called Dvali-Gabadadze-Porrati models produce infrared modification with extra-dimensional gravity dominating at low energy scales [68]. Perhaps the most popular of these models are the "warped braneworld" models [69–73] that generate ultraviolet modification to general relativity with extra-dimensional gravity dominating at high energy scales and address the hierarchy issue in the fundamental scales of physics. These models feature a nonfactorizable curved 5D spacetime, where the 4D metric is a function of the additional dimension through a warping factor.

Attempts to build wormhole models in higher-dimensional spacetime have began to appear recently [74–79]. Kar [80] has proposed a 5D warped wormhole model where the warping chosen is largely inspired by the nonstatic Witten bubble. Recently, in [81], an EB spacetime embedded (with a decaying warp factor) in 5D warped bulk (5D-WEB) is constructed that is supported by on-brane positive energy density matter. Though the weak energy condition is violated, the degree of violation could be made arbitrarily small. We further analyzed the timelike trajectories and the geodesic congruences in these spacetimes in detail in [82,83]. The warping factor, we assume, is that of the well-known thick brane model [84–87], which is a smooth function of the extra dimension (thus there are no derivative jumps or δ functions in the curvature and connections).

In this work, we determine the QNFs (using multiple techniques/algorithms) for both the 4D-(G)EB and 5D-WEB spacetimes and contrast them to distinguish the effects or signatures of the wormhole parameters and the warped extra dimension. The following is a breakdown of the content of this article. In Sec. II, we briefly introduce the novel 5D-W(G)EB wormhole geometry alongside its 4D counterpart. In Sec. III, the field equation for (scalar) perturbation of the geometry and corresponding effective potentials are derived. In Sec. IV, we discuss various methods to solve the master equation in order to determine the time domain profile of the perturbation and QNFs. In Sec. V, we report the results and compare 4D and 5D models to distinguish the signature of the warped extra dimension and the wormhole parameters. Remarkably, we found two distinct QNM eras with two different dominant QNFs. Finally, in Sec. VI, we summarize the work done and key results.

II. 4D-GEB AND 5D-W(G)EB SPACETIME

A 4D-EB wormhole is a spacetime geometry constructed in the presence of a phantom matter field—one whose action contains a negative kinetic energy term. This solution is a spherically symmetric, static, and geodetically complete, horizonless manifold that has a throat (which becomes apparent in an embedding diagram [7]) linking two asymptotically flat regions and is given by the following line element:

$$ds^2 = -dt^2 + \frac{dr^2}{1-\frac{b_0^2}{r^2}} + r^2 d\theta^2 + r^2 \sin^2\theta d\phi^2. \tag{1}$$

Here b_0 is the wormhole's throat radius. The EB spacetime metric can also be written as

$$ds^2 = -dt^2 + dl^2 + r^2(l)d\theta^2 + r^2(l)\sin^2\theta\, d\phi^2, \tag{2}$$

$$\text{with} \quad r^2(l) = l^2 + b_0^2, \tag{3}$$

and l is called the "tortoise coordinate" or proper radial distance. A generalization of the EB model (GEB) is proposed in [35] (which is consistent with Morris-Thorne conditions essential for a Lorentzian wormhole), given by

$$ds^2 = -dt^2 + \frac{dr^2}{1-\frac{b(r)}{r}} + r^2 d\theta^2 + r^2 \sin^2\theta\, d\phi^2, \tag{4}$$

$$\text{with} \quad b(r) = r - r^{(3-2n)}(r^n - b_0^n)^{(2-\frac{2}{n})}. \tag{5}$$

The parameter n takes only even values so that $r(l)$ is smooth over the complete range of $-\infty < l < \infty$. For $n = 2$, we get the original EB geometry back. The GEB metric looks much simpler in terms of the tortoise coordinate,

$$dl^2 = \frac{dr^2}{1-\frac{b(r)}{r}} \Rightarrow r(l) = (l^n + b_0^n)^{\frac{1}{n}}. \tag{6}$$

Note that at the wormhole throat ($l = 0$) the sole nonvanishing derivative is the nth-order derivative of $r(l)$. The effective potential (elaborated later on) also has a nonzero nth derivative at $l = 0$, which gives a negative value for the EB model ($n = 2$ case), while for all other n values it provides a positive value.

The 5D warped Ellis-Bronnikov model, introduced in [81] is

$$ds^2 = e^{2f(y)}[-dt^2 + dl^2 + r^2(l)\,(d\theta^2 + \sin^2\theta d\phi^2)] + dy^2. \tag{7}$$

In this model, y is an extra dimension ($-\infty \le y \le \infty$), $f(y)$ is a warp factor, and the term in square brackets is the GEB spacetime. We assume, $f(y) = \pm\log[\cosh(y/y_0)]$,[1] which

[1]For all numerical calculations, we have chosen $y_0 = 1$.

represents known thick brane solutions in the presence of bulk matter fields [84]. This choice also avoids jumps or δ functions in connections and Riemann tensors. In [81], we showed that for this class of models two of the (on-brane) weak energy conditions, $\rho > 0$ and $\rho + p > 0$, are satisfied in the presence of a decaying warp factor. Further, instead of having $n > 2$ in 4D-GEB, having a warped extra dimension as in the 5D-WGEB model, removes the negative energy density matter completely from the 3-brane located at $y = 0$ [82,83]. The weak energy condition violation comes from radial pressure τ as

$$\rho(l, y) + \tau(l, y) = -2e^{-2f(y)} \frac{r''(l)}{r} < 0 \tag{8}$$

and is negative everywhere. This term can be made arbitrarily small in the $b \to 0$ limit and one may then assume quantum effects to justify such violation. Note that, for a decaying warp factor, the prefactor has its minimum value at the location of the brane only.

III. FIELD EQUATION AND EFFECTIVE POTENTIAL

The perturbations or fluctuations in a black hole or wormhole geometry may be caused by merger or gravitational interactions with other astrophysical objects or even the so-called test objects that may represent a spaceship passing through. The scalar frequencies of these perturbations evolve via a massless Klein-Gordon equation, given by

$$\nabla_\mu \nabla^\mu \Psi = \frac{-1}{\sqrt{-g}} \partial_\mu \left(g^{\mu\nu} \sqrt{-g} \partial_\nu \Psi \right) = 0, \tag{9}$$

where Ψ is the scalar (field) perturbation and g is the determinant of the metric tensor involved. For massive scalar field perturbation with mass m, the right-hand side of Eq. (9) will carry a term $m^2\psi$. This equation does allow (with appropriate boundary conditions) solutions having complex frequencies. These QNFs have a natural interpretation as gravitational radiation where the black hole/wormhole is treated as an open system. The QNFs, by definition, are associated with specific boundary conditions which says they are purely outgoing waves at spatial infinities. The real part of a QNF denotes the oscillation, while the imaginary part implies damping of the field over time. The vector and tensor perturbations (wherever applicable) also follow a similar field equation as scalar frequencies as such. These QNFs are also key to testing stability of a wormhole geometry under perturbation. They certainly depend on the various wormhole parameters involved and thus could have distinct features in comparison with black holes as such. Analysis of the effective potential and determination of QNFs for the 4D-GEB model are briefly addressed in [36]. Below we reproduce and extend their result of the 4D scenario and then compare them with the corresponding results derived for 5D-WEB spacetime.

A. 4D scenario

Since the wormhole geometry is static and spherically symmetric, one may use the following separation of variables for the field Ψ, in the 4D-GEB scenario, as

$$\Psi(t, r, \theta, \phi) = \mathcal{Y}(\theta, \phi) \frac{R(r) e^{-i\omega t}}{r}, \tag{10}$$

where $\mathcal{Y}(\theta, \phi)$ are the spherical harmonics. This leads to a form similar to the Schrödinger equation in the tortoise coordinate l,

$$\omega^2 + \frac{1}{R} \frac{\partial^2 R}{\partial l^2} - V_{\text{eff}} = 0. \tag{11}$$

The "effective potential" V_{eff} is given by

$$V_{\text{eff}} = \left[\frac{(n-1) b_0^n l^{n-2}}{(l^n + b_0^n)^2} + \frac{m(m+1)}{(l^n + b_0^n)^{2/n}} \right], \tag{12}$$

where m represents the azimuthal angular momentum. In terms of the radial coordinate, the effective potential is simply

$$V_{\text{eff}} = \left[\frac{r''}{r} + \frac{m(m+1)}{r^2} \right]. \tag{13}$$

Before going into the solutions of the field equation and determination of the QNFs, let us analyze the effective potential corresponding to perturbations in 4D and 5D models.

Figure 1 shows the variation of the effective potential versus l for the various 4D-GEB models (varying n) for four different angular frequencies $m = 1, 2, 5, 10$; whereas the plots in Fig. 2 show the variation of effective potential versus l for $n = 2$ (EB case) and $n = 4$ (for various m frequencies).[2] A few prominent features observed from these plots are as follows.

(i) V_{eff} exhibits a single barrier for $n = 2$, while a twin barrier exists for all $n > 2$. This particular feature, in fact, corresponds to removal of the exotic matter from the throat region.

(ii) For higher m frequencies, the potential increases and for $n > 2$, twin peaks merge to create a plateau-shaped single barrier. In other words, the twin barrier feature is only visible for low values of m. This could have important implications for the stability of the 4D-GEB model which may be addressed elsewhere.

[2]The throat radius b_0 is taken as unity for numerical evaluation.

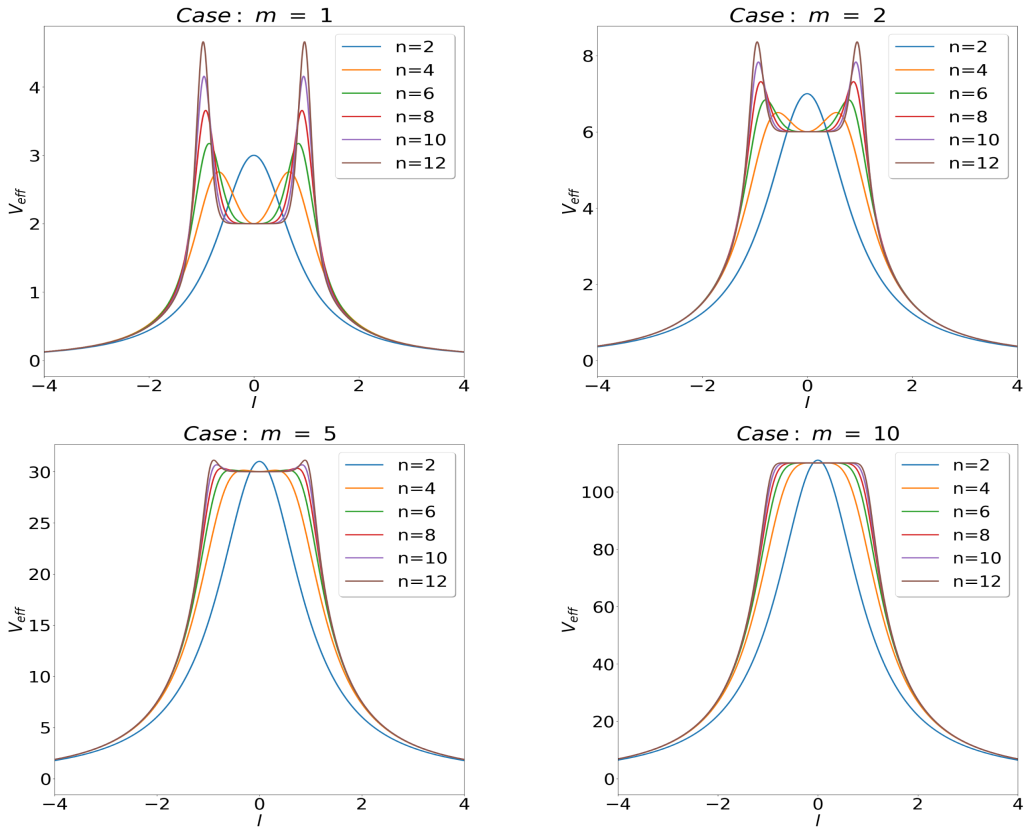

FIG. 1. Plot of effective potential for fixed m and varying n, (top left) $m = 1$, (top right) $m = 2$, (bottom left) $m = 5$, (bottom right) $m = 10$.

(iii) It is known that the WKB method to determine QNFs is not suitable for twin barrier potentials. However, the potential profiles suggest that the WKB formula could be useful even for $n > 2$ for high m.

(iv) All potentials vanish asymptotically which implies trivial boundary condition for QNMs.

B. 5D scenario

In the 5D-WGEB spacetime given by Eq. (7), we use the following separation of variables:

$$\Psi^{5D} = Y(\theta,\phi)e^{-i\omega t}\frac{R(r)}{r}F(y)e^{-f(y)}, \tag{14}$$

where $F(y)$ and $f(y)$ are functions only depending on y. Thus, the Klein-Gordon equation in 5D leads to

$$\left(\omega^2 - \left[\frac{(n-1)b_0^n l^{n-2}}{(l^n+b_0^n)^2} + \frac{m(m+1)}{(l^n+b_0^n)^{2/n}}\right] + \frac{1}{R}\frac{\partial^2 R}{\partial l^2}\right) = -\left[\frac{1}{F}\frac{\partial^2 F}{\partial y^2} + 2\frac{1}{F}\frac{\partial F}{\partial y}\frac{\partial f}{\partial y} - \frac{\partial^2 f}{\partial y^2} - 3\left(\frac{\partial f}{\partial y}\right)^2\right]e^{2f(y)}. \tag{15}$$

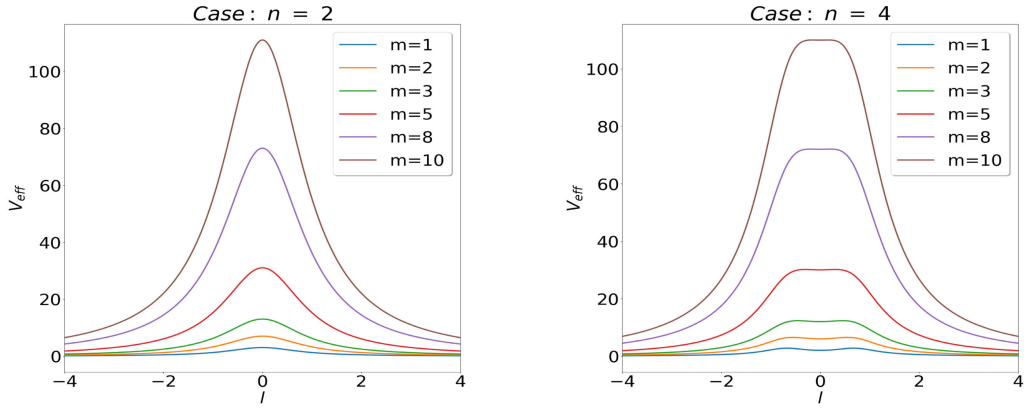

FIG. 2. Plot of effective potential for fixed n and varying m, (left) $n = 2$, (right) $n = 4$.

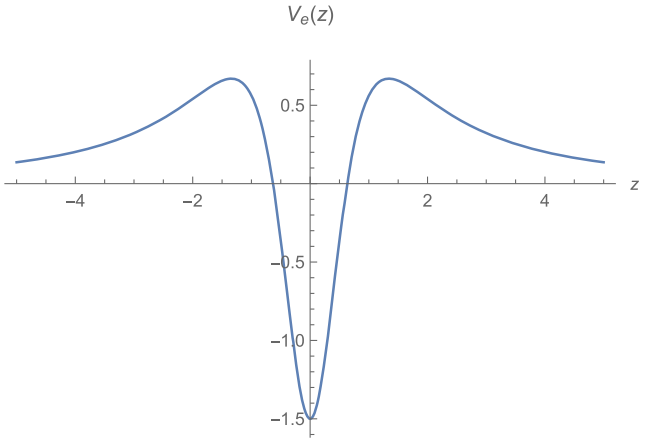

FIG. 3. Plot of potential $V_e(z)$ versus z.

Now taking

$$-e^{2f(y)}\left[\frac{1}{F}\frac{\partial^2 F}{\partial y^2}+2\frac{1}{F}\frac{\partial F}{\partial y}\frac{\partial f}{\partial y}-\frac{\partial^2 f}{\partial y^2}-3\left(\frac{\partial f}{\partial y}\right)^2\right]=q^2, \quad (16)$$

Equation (15) reduces to the form of Eq. (11) with the effective potential being

$$V_{\text{eff}}=\left[\frac{(n-1)b_0^n l^{n-2}}{(l^n+b_0^n)^2}+\frac{m(m+1)}{(l^n+b_0^n)^{2/n}}\right]+q^2. \quad (17)$$

To find the eigenvalues q^2 by solving Eq. (16), let us first do a coordinate transformation given by $dz=dye^{-f}$, i.e., $z=\sinh y$ (for the decaying warp factor), that leads to

$$\frac{\partial^2 F}{\partial z^2}+\frac{\partial f}{\partial z}\frac{\partial F}{\partial z}-\left[\frac{\partial^2 f}{\partial z^2}+2\left(\frac{\partial f}{\partial z}\right)^2\right]F=-q^2F. \quad (18)$$

Then, we use the ansatz $F(z)=G(z)\exp(-f/2)$, leading to the following simpler form:

$$-\frac{\partial^2 G}{\partial z^2}+V_e(z)G=q^2G, \quad \text{where}$$
$$V_e(z)=\frac{3}{2}\frac{\partial^2 f}{\partial z^2}+\frac{9}{4}\left(\frac{\partial f}{\partial z}\right)^2=\frac{3(5z^2-2)}{4(z^2+1)^2}. \quad (19)$$

The potential $V_e(z)$ is plotted in Fig. 3. This potential vanishes as $z\to\pm\infty$, which implies that positive (or real q) eigenvalues are a continuum. This analysis is consistent with numerical solution found using *Mathematica*. Apparently, it may seem that for negative eigenvalues a discrete spectrum exists. This can be investigated with the following approximation. The series expansion of the potential about $z=0$ is given by

$$V_e(z)=-\frac{3}{2}+\frac{27}{4}z^2-12z^4+\frac{69}{4}z^6-O(z)^8, \quad (20)$$

since, for the negative part of the potential $|z|<1$, we choose to ignore the terms of $O(z)^4$ onward. This leaves us with a harmonic oscillator potential whose eigenvalues are given by

$$E_{h.o.}=\left(n+\frac{1}{2}\right)\sqrt{27}-3/2, \qquad n=0,1,2.... \quad (21)$$

The ground state eigenvalue, for $n=0$, is positive in spite of the factor $-3/2$. This observation remains unchanged if we include higher-order terms and find the eigenvalue numerically. Thus, there are no negative eigenvalues or bound states of Eq. (19).[3] Thus, the q^2-term effectively contributes as an effective mass in the Schrödinger equation. This is a well-known feature of massless 5D field equation when projected on 4D as such. Thus, the potential given by Eq. (17) is equivalent to the potential of the massive scalar field with mass q in the 4D-GEB (or pure EB) background. However, no such studies could be found in the literature, which makes it difficult compare our result with previous results. One can say that Eq. (17) is unique and results in unique signature QNMs, as we are going to see in what follows. A somewhat similar effective potential appears in the presence of a massive scalar field in a 4D black hole background [88,89]. There, authors have shown that, for some values of the black hole mass and the scalar field mass, purely real QNM frequencies or the so-called quasiresonances exist.[4] We shall see similar results below. Horowitz and Hubeny [90] have addressed a similar problem in the sense that we also have an asymptotically nonvanishing potential (see Fig. 4). Note that the effect of the extra dimension is encoded in the eigenvalues q^2. If q^2 takes continuous values, then the information about the functional from the warp factor would not be imprinted on the QNFs to be determined below.

In what follows, we shall choose suitable values of q to be put in Eqs. (11) and (17) for numerical evaluation and graphical presentations. Note that q has a dimension of inverse length. Therefore, its exact numerical value is less important for our purpose. So, one can set $y_0=1$ without losing any generality. However, "$q=b_0^{-1}$" is expected to have a physical significance as we will see later.

Figure 4 shows the effective potential profile versus l, for various values of q with fixed azimuthal angular momentum ($m=2$) for $n=2$ (WEB) and $n=4$ (a WGEB) geometries. Due to the presence of the extra dimension, as $l\to\infty$, the potential does not vanish and essentially becomes equal to q^2, consistent with Eq. (17). This will be

[3]Negative eigenvalues would imply imaginary q values.
[4]Naturally, there is a debate whether these frequencies can be called QNFs at all.

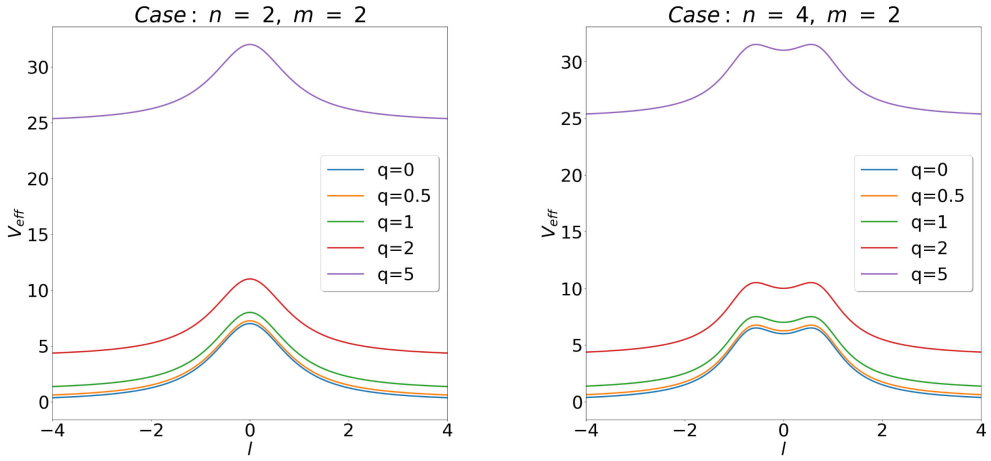

FIG. 4. Plot of effective potential for constant m and n at different dimensions (varying q), (left) $n = 2$, $m = 2$; (right) $n = 4$, $m = 2$.

reflected in the choice of boundary conditions to determine the QNFs using various methods.

IV. TIME DOMAIN SPECTRUM AND QUASINORMAL FREQUENCIES

WGEB models with a decaying warp factor satisfy the energy conditions even for $n = 2$ or the original EB spacetime [81] where there is a single barrier only; which, in turn, suggests that one may use the WKB method to find approximate QNF values, not only for 4D-EB wormholes, but also for 5D-WEB ($n = 2$) wormholes as well. We employ numerical methods to supplement the WKB approach also for higher accuracy in cases where the WKB approach is less efficient.

A. WKB approach

The semianalytical WKB approximation to derive QNFs was developed by Schutz and Will [91]. The method is based on matching of the asymptotic WKB solutions at spatial infinities and at the neck of the wormhole (event horizon in the case of a black hole) with the Taylor expansion near the top of the potential barrier through the two turning points. The QNFs found by taking the WKB solutions up to the eikonal limit are given by the following formula [92,93]:

$$w_p^2 = V_0 - i\left(p + \frac{1}{2}\right)\sqrt{-2V_0''}, \tag{22}$$

where V_0 and V_0'' denote the values of the effective potential and its second derivative at the maximum. p denotes the overtone number, with $p = 0$ being the fundamental mode. For our model, Eq. (22) implies (for $n = 2$ scenario)

$$w_p^2 = \frac{m^2+m+1}{b_0^2} + q^2 - 2i(2p+1)\frac{\sqrt{m^2+m+2}}{b_0^2}. \tag{23}$$

It is straightforward to show that, for large effective mass $q \gg m$, we get purely real $w_p \sim q$ or the so-called quasiresonances, which were reported for wormholes in [94]. Numerical results will show more details. Here, we focus only on the fundamental frequencies and compare the WKB values with the numerical results (derived in the next section) in the tables given below. For a recent comprehensive review on WKB methods, one may refer to [48]. Let us now discuss the numerical methods to compute the QNFs for 4D and 5D geometries.

B. Numerical approaches

QNFs are complex frequencies that characterize damped oscillation of gravitational perturbations in the metric. There are many methods developed to determine these frequencies. Few numerical approaches are designed to find QNFs with any desired accuracy (see [48] for a review of methods), which are based on convergent procedures. Each has its own advantages and disadvantages. Developing efficient methods to compute QNFs is an active area of research. The analytic methods, e.g., WKB method, are less accurate compared to numerical methods, for example, in the presence of multiple barriers (e.g., $n > 2$ in GEB models) [36]. The time-dependent wave equation, integrated over the angular coordinates, has following form:

$$V_{\text{eff}}\Psi_m(t,l) + \frac{\partial^2\Psi_m(t,l)}{\partial t^2} - \frac{\partial^2\Psi_m(t,l)}{\partial l^2} = 0. \tag{24}$$

In the first method, we determine the time evolution of the scalar perturbation by numerically integrating Eq. (24) using the methodology presented in [48,95]. The essential steps are as follows. One first adopts the light cone coordinates, $du = dt + dl$ and $dv = dt - dl$, which implies

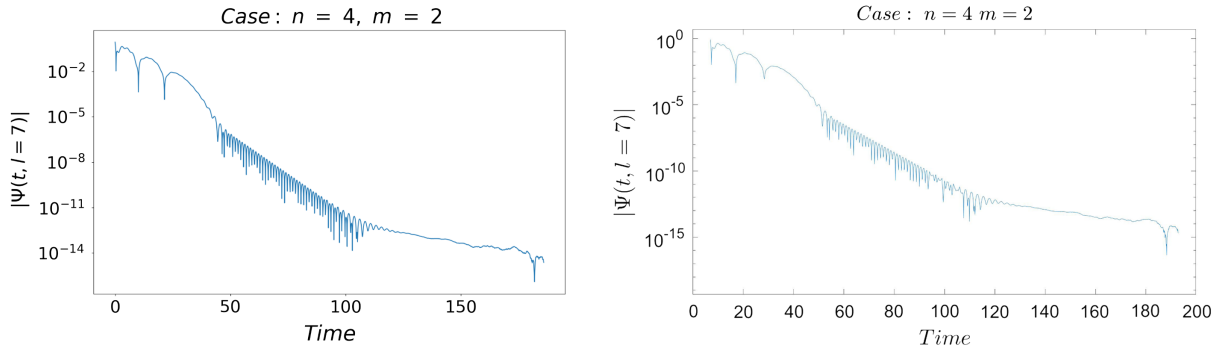

FIG. 5. Time domain spectrum for $n = 4$, $m = 2$, using PYTHON (left) and MATLAB (right).

$$\left(4\frac{\partial^2}{\partial u\partial v} + V_{\text{eff}}(u,v)\right)\Psi_m(u,v) = 0. \tag{25}$$

The time evolution operator, using simple two-variable Taylor expansion, reads as

$$\begin{aligned}\exp\left(h\frac{\partial}{\partial t}\right) &= \exp\left(h\frac{\partial}{\partial u} + h\frac{\partial}{\partial v}\right)\\ &= -1 + \exp\left(h\frac{\partial}{\partial u}\right) + \exp\left(h\frac{\partial}{\partial v}\right)\\ &\quad + \frac{h^2}{2}\left[\exp\left(h\frac{\partial}{\partial u}\right) + \exp\left(h\frac{\partial}{\partial v}\right)\right]\frac{\partial^2}{\partial u\partial v} + \mathcal{O}(h^4),\end{aligned} \tag{26}$$

where h is the step size. Thereafter, we numerically integrate over du and dv, ideally in the range $[0,\infty]$. We have computed the field amplitude in the region $0 \le u, v \le 200$ with a step size $h = 0.01$. The initial condition is taken as a Gaussian distribution along $v = 0$, $\Psi(u,0) = e^{\frac{-(u-10)^2}{100}}$, and as a constant along $u = 0$, $\Psi(0,v) = 1/e$, such that they equate at $\Psi(0,0)$. This computation is performed using both PYTHON and MATLAB to cross-check for accuracy. A particular case, with $n = 4$, $m = 2$ in the 4D-GEB model, is shown in the (log-linear) plots in Fig. 5. This shows that the efficiency of the two computing platforms is comparable. The presence of quasinormal frequencies is clearly evident from these time domain evolution spectra.

From the log-linear plots in Fig. 5, one may identify three distinct stages in the time domain spectrum the initial region, approximately for tenure $t = 0$–50 s (which depends on the initial condition), the second stage, the region of our interest—the exponential dampening—roughly during $t = 50$–110 s, followed by the third stage of "tail" [48,95]. Note that with increase in b_0 value the duration quasinormal ringing increases, which suggests a decrease in the value of the QNF. This feature is also present in the 5D scenario. In fact, this can be seen by straightforward evaluation of the WKB formula, Eq. (22). From the damped region one can extract the QNF values by the "Prony fitting" method (discussed below). We have also used the "direct integration" method to determine the QNFs. Below, we briefly discuss these methodologies followed by the tabulated results.

C. Determination QNFs

1. Prony method

In the Prony method, the time domain profile is fitted by the function

$$f(t) = \sum_{n=0}^{\infty} A_n e^{\alpha_n t}\cos(\beta_n t), \tag{27}$$

where the QNFs are given by $\omega_{\text{QNF}} = \alpha \pm i\beta$. This technique is similar to the Fourier method but is also valid for complex frequencies and was first developed by Prony in 1795 [48]. There is another variation of this technique [50], where the function is equated with the time domain spectrum and converted into a matrix form whose roots (eigenvalues) are found to be the QNFs. This technique is used in all fields having any damped oscillatory signal processing. We used both of these approaches for reliability (using both PYTHON and MATLAB). An example of the Prony fitting is depicted in Fig. 6.

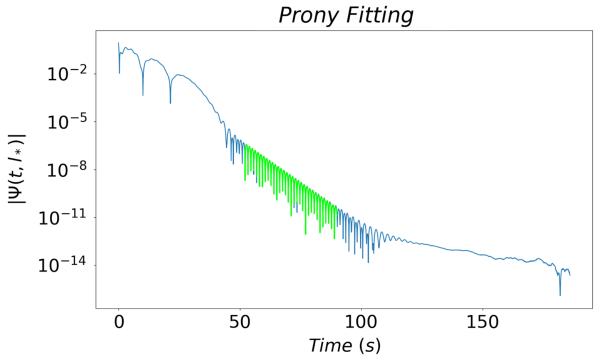

FIG. 6. Time domain spectrum fit with dominant ω_{QNF} for $n = 4$, $m = 2$ using PYTHON.

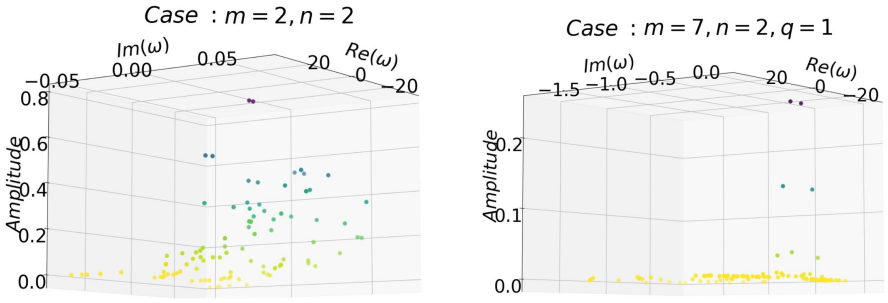

FIG. 7. Amplitudes A_n of fitting frequencies with dominant $\omega_{\rm QNF}$ having the greatest value.

The matrix (Prony) method returns a set of complex frequencies which are further analyzed and sorted with respect to a magnitude similar to the Fourier technique. In Fig. 7, we graphically present the amplitude of each mode obtained in the matrix method (using Python). It is evident that only two frequencies (conjugate of each other) have the highest magnitude and hence are the most dominating. Thus, the QNFs in their order of dominance can be identified. We shall not show the amplitude plots for any other cases for brevity.

2. Direct integration

In the direct integration method, the characteristic or the master differential equation (11) is numerically integrated using purely outgoing boundary conditions. This technique was first used by Chandrasekhar and Detweiler [96] in 1975. We essentially follow the steps described in [36,97]. As our potential is symmetric about the wormhole throat ($l = 0$) (in both 4D and 5D cases) our solution can be of the symmetric or antisymmetric kind. For the symmetric (antisymmetric) solution, we should use $R'(0) = 0$ ($R(0) = 0$). Note that the asymptotic solution near $l \to \infty$ can be expanded as

$$R^{+} = e^{i\Omega l}\sum_{k=0}^{\infty}\frac{A_k^{+}}{l^k}; \qquad \Omega^2 = \omega^2 - q^2, \tag{28}$$

which represents a purely outgoing wave. However, near the throat or at some finite distance from the throat, expansion should contain both ingoing and outgoing waves, given by

$$R(l) = e^{i\Omega l}\sum_{k=0}^{\infty}\frac{A_k^{+}}{l^k} + e^{-i\Omega l}\sum_{k=0}^{\infty}\frac{A_k^{-}}{l^k}. \tag{29}$$

By putting $R(l)$ in the field equation, one gets the following recurrence relations (at large $l_0^2 \gg b_0^2$):

$$A_{k+1}^{\pm} = \pm\frac{\{k(k+1) - m(m+1)\}A_k^{\pm} + (n-1)b_0^n A_{k-n}^{\pm}}{2i\Omega(k+1)}. \tag{30}$$

This gives all the $A_k^{\pm}$ in terms of $A_0^{\pm}$. After we integrate Eq. (11) from $l = 0$ to $l = l_0$, we match the numerically found $R_{\rm num}(l)$ and $R'_{\rm num}(l)$ with Eq. (29) and its derivative at l_0. This leads to the following matching conditions:

$$R_{\rm num}(l_0) = e^{i\Omega l_0}\sum_{k=0}^{\infty}\frac{A_k^{+}}{l_0^k} + e^{-i\Omega l_0}\sum_{k=0}^{\infty}\frac{A_k^{-}}{l_0^k}, \tag{31}$$

$$R'_{\rm num}(l_0) = e^{i\Omega l_0}\sum_{k=0}^{\infty}\frac{A_k^{+}}{l_0^k}\left(i\Omega - \frac{k}{l_0}\right) + e^{-i\Omega l_0}\sum_{k=0}^{\infty}\frac{A_k^{-}}{l_0^k}\left(-i\Omega - \frac{k}{l_0}\right). \tag{32}$$

Eliminating A_0^{+} from Eqs. (31) and (32), we get an expression of A_0^{-} as a function of l_0 and ω. Roots of the equation $A_0^{-} = 0$, in the large l_0 limit, gives us the QNFs. The stability of the solutions is checked by verifying that varying l_0 does not considerably change the QNF values. We have only considered QNFs corresponding to the symmetric solutions, which have low damping.

V. RESULTS

Our focus will be on $n = 2$ or the pure EB model as we are going to compare these results with the 5D scenario. However, we will also address higher n geometries (4D-GEB) briefly for completeness and to extend the results presented in [36].

A. 4D wormhole: Varying n and m

Figure 8 shows that for the 4D-EB wormhole ($n = 2$) the damped oscillatory region is less prominent for lower values of m. Therefore, QNF values extracted from these evolutions, using Prony fitting, are sensitive to the choice of beginning and end of QNM oscillation.

Figure 9 shows time evolution for a "steep-neck" 4D-GEB geometry with $n = 10$ (for $m = 2$) and $n = 4$ (for $m = 5$). Comparison with Fig. 5 shows that, with increasing n, the beginning of the quasinormal ringing domain has not changed much, but the end is delayed considerably, i.e., the tail appears much later for a higher value of n. Whereas with increasing m, the QNM oscillation gets triggered

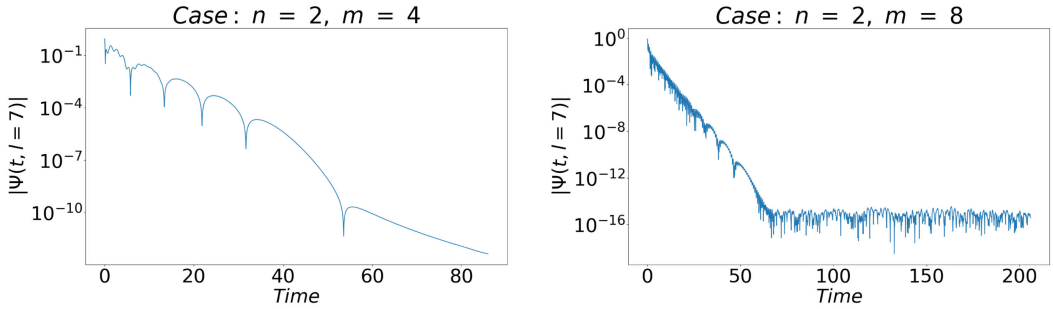

FIG. 8. Time domain spectrum for $n = 2$, $m = 4$ and $n = 2$, $m = 8$.

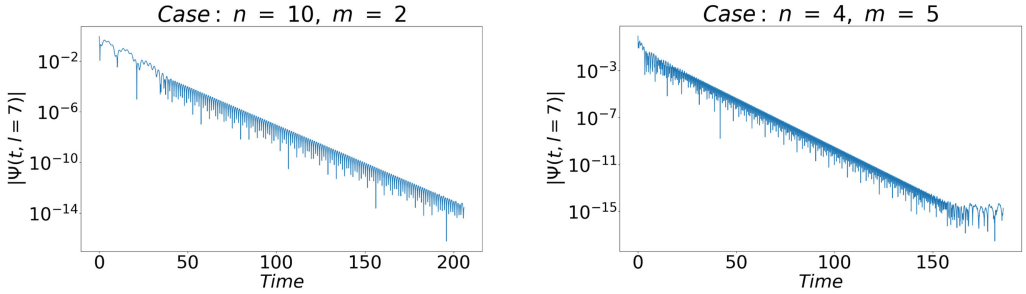

FIG. 9. Time domain spectrum for $n = 10$, $m = 2$ and $n = 4$, $m = 5$.

earlier. These particular features could be a useful signature in detecting the shape of the GEB wormholes apart from those reported in [36].

The (dominant) quasinormal frequencies for various m (angular momentum) and n (steep-neck parameter) values in 4D-GEB have been plotted (real versus the absolute value of imaginary) in Fig. 10. We clearly see that the features of $n = 2$ are markedly different from the $n > 2$ scenario. Figure 10 essentially reproduces results found in [36] and establishes the accuracy of our numerical computation. For a detailed discussion on Fig. 10, we urge the reader to consult [36].

B. 5D wormhole: $n = 2$, varying m and q

In the context of the 5D model, as argued earlier, we focus on the $n = 2$ scenario. Incidentally, the effects of the extra dimension (i.e., of varying q value or the *massiveness* coming from the warped extra dimension) on the time evolution is more striking for higher values of m. Let us look at the time domain profile for $n = 2$, $m = 8$ (any other value of m will do) with varying q values. Figure 11 shows the remarkable changes in the time evolution profile of the wave amplitude for four different values of q.

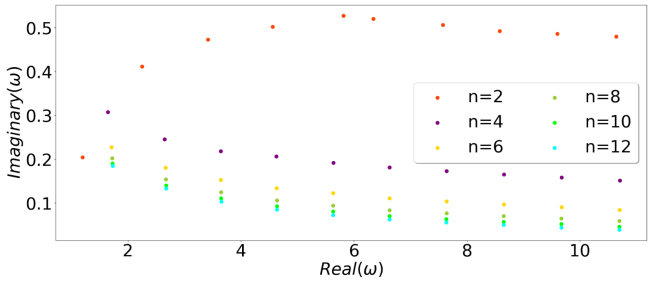

FIG. 10. Plot of ω_{QNF}, real versus (magnitude of) imaginary part for different n and m values. From left to right, the m value increases.

Even for small (but nonzero) values of $q = 0.5$, the 4D behavior (which is equivalent to setting $q = 0$) is lost. This is expected as there is an interplay between m and q. Interestingly, for $q > b_0^{-1}$ (here we have taken $b_0 = 1$), the semilog plots clearly reveal that the QNM era is divided into *two* parts (almost as if two linear regions with different slopes are joined at a kink) that are dominated by two different QNF modes. Notably, in the latter region, the most dominant QNM is characterized by $\mathrm{FFF}(\omega) \sim q$ with a small imaginary part as depicted in the tables given below. As time evolves, eventually, when the early dominant modes decay, the late QNM emerges. To further reveal the late QNM region, we present Fig. 12. Here, in the left plot we show a perfect fit of the early QNM region using the dominant QNF found to be $\omega^{(E)} = 5.335 + i0.41$. In the right plot, we have fitted the wave amplitude, after subtracting that dominant early QNM, with the dominant late QNM given by $\omega^{(L)} = 2.0078 + i0.0043$. The order of their dominance has also been confirmed from their amplitudes using the matrix Prony method as mentioned earlier. The (almost) purely real frequencies, in the late QNM era, are similar to the quasiresonances found in [88,98]. Though the imaginary part is nonzero but very

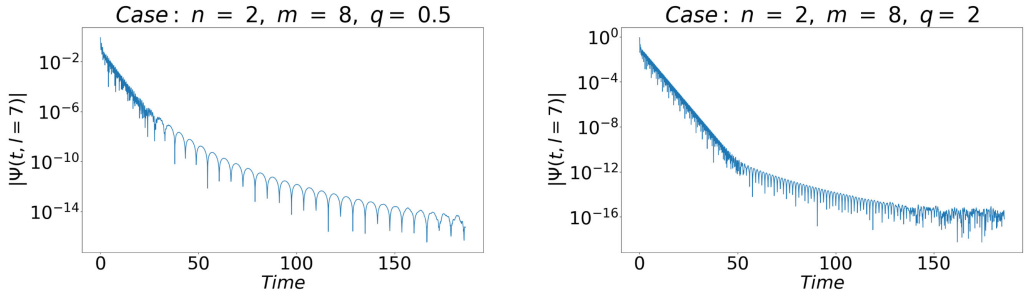

FIG. 11. Time domain spectrum for $n = 2$, $m = 8$, and $q = 0.5$ (left), $q = 2$ (right).

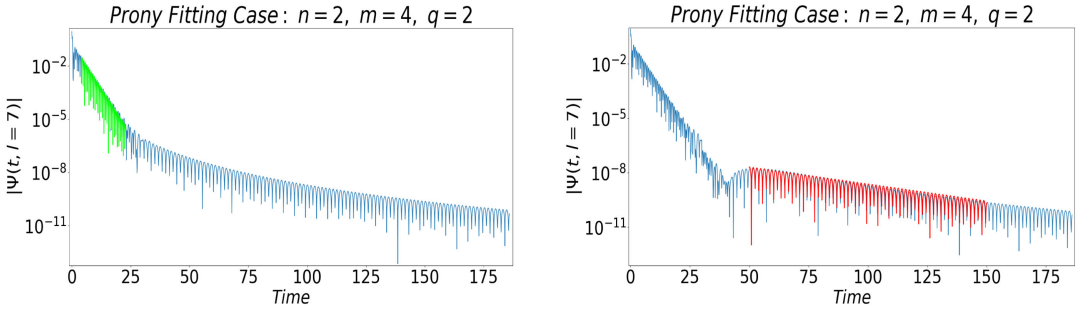

FIG. 12. Time domain spectrum and dominant QNM fit at early (left) and late (right) QNM era.

small for the QNMs we report here, it is easy to see that (from Tables I and II), for larger and larger q, the imaginary part indeed tends to zero and we have exact quasiresonances. Note that it is not the existence of the quasiresonances, but the existence of two QNM eras, where the *late* QNM region is dominated by the almost quasiresonant QNM, that we emphasize as the signature of the warped extra dimension in the ringing of an effective 4D-EB wormhole.

In Tables I and II, we tabulated early and late dominant QNFs, respectively, for $n = 2$, various q momentum, and angular momenta m, determined using different methods.

TABLE I. Early time dominant QNF–$\omega^{(E)}$ values for various modes at $n = 2$.

m	q	Prony	Direct integration	WKB
1	0	0.8 32130 − i0.226690	1.624584 − i0.219350	1.617350 − i0.250251
	0.5	0.750281 − i0.188820	1.851582 − i0.188352	1.879640 − i0.242017
	1	1.335939 − i0.215243	2.053928 − i0.215267	2.058170 − i0.185868
	2	2.621701 − i0.123791	2.621708 − i0.123782	2.672090 − i0.124239
	5	5.396131 − i0.036641	5.396137 − i0.036642	5.394870 − i0.038862
2	0	2.250079 − i0.457395	2.712579 − i0.445679	2.629721 − i0.424325
	0.5	1.505729 − i0.317217	2.810257 − i0.312587	2.741552 − i0.315845
	1	2.528403 − i0.279339	2.948405 − i0.279358	2.871002 − i0.282586
	2	3.195762 − i0.231845	3.194526 − i0.221053	3.343490 − i0.222976
	5	6.089024 − i0.304504	6.129243 − i0.315208	6.171861 − i0.303122
5	0	5.590286 − i0.527592	5.582526 − i0.512567	5.590768 − i0.505916
	0.5	5.608272 − i0.515912	5.611273 − i0.518386	5.612845 − i0.503921
	1	5.732418 − i0.514532	5.727413 − i0.503953	5.678741 − i0.498073
	2	5.913451 − i0.477296	5.922475 − i0.476795	5.935240 − i0.476548
	5	7.480281 − i0.367137	7.480376 − i0.369172	7.492832 − i0.377485
8	0	8.579942 − i0.492730	8.529875 − i0.491728	8.558772 − i0.492544
	0.5	8.621930 − i0.486822	8.624282 − i0.482853	8.573310 − i0.491692
	1	8.643952 − i0.481875	8.647258 − i0.484326	8.616820 − i0.489164
	2	8.979098 − i0.468332	8.979096 − i0.478331	8.788610 − i0.469402
	5	9.979701 − i0.312355	9.978305 − i0.327316	9.90901 − i0.324066

TABLE II. Late time dominant QNF–$\omega^{(L)}$ values for various modes at $n = 2$.

m	q	Prony	Direct integration
1	0.5	$0.507324 - i0.030946$	$0.507425 - i0.030862$
	1	$1.001504 - i0.017169$	$1.001248 - i0.017066$
	2	$2.008260 - i0.003081$	$2.008267 - i0.003019$
	5	$5.030260 - i0.000004$	$5.030188 - i0.000009$
2	0.5	$0.513874 - i0.055556$	$0.512767 - i0.055676$
	1	$1.004001 - i0.014508$	$1.005080 - i0.014216$
	2	$2.009095 - i0.004750$	$2.008207 - i0.004302$
	5	$5.036428 - i0.000003$	$5.035281 - i0.000002$
5	0.5	$0.525911 - i0.122378$	$0.525908 - i0.122350$
	1	$1.016924 - i0.037482$	$1.016979 - i0.039472$
	2	$2.006454 - i0.008466$	$2.006424 - i0.008492$
	5	$5.004510 - i0.000001$	$5.004522 - i0.000002$
8	0.5	$0.504295 - i0.156266$	$0.504383 - i0.156142$
	1	$1.032865 - i0.036472$	$1.030675 - i0.036488$
	2	$2.001427 - i0.001418$	$2.001445 - i0.001433$
	5	$5.004831 - i0.000000$	$5.004853 - i0.000000$

For brevity, we have denoted the early dominant QNF as $\omega^{(E)}$ and the late dominant QNF as $\omega^{(L)}$. Note that the WKB method only matches with early QNMs.

In Table I, the QNF values for $q = 0$ do match up to three digits after the decimal point with the 4D-GEB QNF values reported in [36], thus proving the accuracy of our numerical computation. The Prony method fails to provide accurate determination of early QNFs for low m values because of small duration. However, using larger numerical value for b_0, duration increases and the Prony method gives better results for low m values as well. Also, as q increases, accuracy improves. For nonzero q, the dominant QNF in the early QNM era gets larger with increasing q. Table II shows that, as the q value increases, the imaginary part of the fundamental mode tends to zero asymptotically while the real part approaches q. Apparently, from Eq. (17), this behavior is expected if one takes the $q \gg m$ limit. Figure 13 shows how the real and the imaginary part of the QNF varies with varying q.

Note that in [88] it was found that, for massive scalar fields in the black hole background, quasiresonance is achieved above a certain threshold value of the mass, whereas we are getting similar behavior in the $q \to \infty$ limit. Further, the short-lived early QNM era was also not reported there. It is crucial to identify the duration of the QNM era to determine accurate values of QNF. Note that, for low angular momentum values m, the duration of the early QNM era is small and thus difficult to detect. Therefore, one might guess that, even in the case of a massive scalar field, there exists an early QNM era. However, we did look at the time domain profiles in detail for massive perturbation of black holes, but did not find such behavior. Coming back to our model, for $q < b^{-1}$, the duration of early QNM decreases indefinitely with decreasing q. For such low values of q, the time span of the dominant QNF in the early QNM era becomes smaller than our algorithm's precision limit in the Prony method. This limitation does not show up for the other methods so they generate efficient values for QNF in those cases.

VI. DISCUSSION

The Ellis-Bronnikov wormhole (and its generalized versions) embedded in warped braneworld background has been shown to be supported by positive energy density matter in the presence of a decaying warp factor. The violation of the weak energy condition can be minimized arbitrarily. Earlier we have studied particle trajectories and geodesic congruences in such spacetimes. The recent observations suggest that one way to understand the true nature of the ultracompact objects is through their quasinormal ringing. This method could potentially distinguish among black holes and possible black hole mimickers such as wormholes. Here we analyze the QNMs of the 5D-WEB wormhole spacetime while looking for distinguishing features of the warped extra dimension and the wormhole parameter. The work done and the results found reveal the effects of the warped extra dimension (through effective mass q) and the wormhole (steep-neck) parameter n on the time domain profile and the QNFs. We summarize the key findings below in a systematic manner.

(i) The nature of the effective potential is almost similar in both four and five dimensions, with a crucial

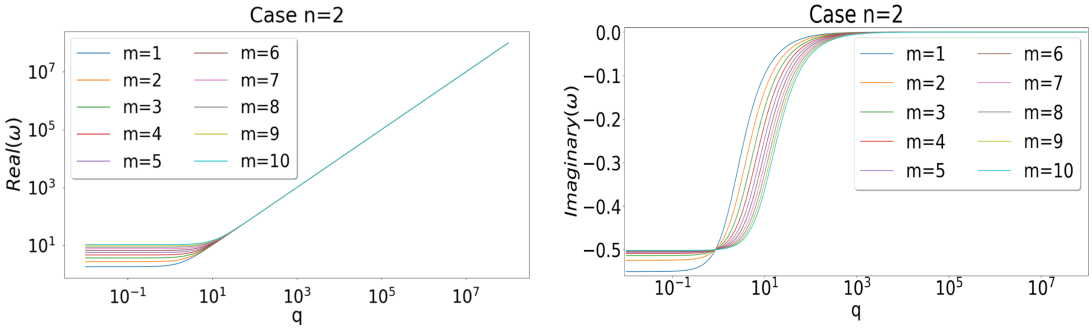

FIG. 13. Plot of Re(QNF) and Im(QNF) for $n = 2$ with varying q and m.

difference that, in 5D, the potential does not vanish asymptotically.

(ii) The momentum eigenvalue along the fifth dimension q, projected on the 4D geometry, acts as an effective mass. We solved the corresponding eigenvalue problem and found that q takes non-negative continuous values.

(iii) Assuming suitable values of q, we then determined the QNFs analytically using the WKB formula and numerically using the Prony method and the direct integration method. The results for the 4D-GEB model match to third decimal order with earlier reports. We have used both Python and MATLAB for numerical computation of QNFs.

(iv) For 4D-GEB spacetimes, the time domain profile has three prominent regions (the initial portion, the QNM era, and an asymptotic tail. Apart from the observations made in [36], we notice that the QNM ringing appears earlier for higher angular momentum m and the tail appears later for higher values of n.

(v) Remarkably, the time domain profile changes considerably in the 5D-WEB scenario. The QNM era is divided into two parts with two different dominant QNFs. The real part of the "early QNM" (for fixed m) increases with increasing q value, whereas the real part of the "late QNM" is close to the q value. Also, the dampening (decided by the imaginary part of the QNF) of the late QNM is much slower than that of the early QNM.

(vi) With increasing q, the late QNM eventually becomes arbitrarily long-lived. This arbitrarily long-lived mode emerges once the dominant (early) QNM decays away. These so-called quasiresonances were observed earlier for massive fields in black hole backgrounds. Further, the tail appears much later compared to the 4D scenario.

Note that the novel feature that could be seen in the time domain profile of the perturbation is not of quantitative or parametric type. There are *two* QNM eras observed, instead of one, whose durations naturally vary for varying q. We believe such behavior is predicted or reported in the literature for the first time. Hence, one may conclude that this feature of two different dominating QNFs in the ringing profile, if observed, could provide indirect evidence of existence (though not conclusive) of wormholes, as well as five-dimensional warped geometry. It is always difficult to build physical intuition about the nature of the QNMs once they are determined numerically. However, we have seen that it is the interplay between m and q that is responsible for the splitting of the QNM era. Further, one might find similar splitting in other equivalent and preferably more generic scenarios. We look forward to report on this in future.

ACKNOWLEDGMENTS

We thank Dr. Poulami Dutta Roy and Professor Sayan Kar for useful discussions and correspondence. S. G. thanks Birla Institute of Technology Mesra for financial assistance through a seed money grant with Grant No. DRIE/SMS/DRIE-05/2023-24/2352.

[1] Matt Visser, *Lorentzian Wormholes: From Einstein to Hawking* (American Institute of Physics, Woodbury, NY, 1995).
[2] Miguel Alcubierre, *Wormholes, Warp Drives and Energy Conditions* (Springer, New York, 2017), Vol. 189, 10.1007/978-3-319-55182-1.
[3] M. D. Kruskal, Maximal extension of Schwarzschild metric, Phys. Rev. **119**, 1743 (1960).
[4] Robert W. Fuller and John A. Wheeler, Causality and multiply connected space-time, Phys. Rev. **128**, 919 (1962).
[5] Douglas M. Eardley, Death of white holes in the early Universe, Phys. Rev. Lett. **33**, 442 (1974).
[6] Robert M. Wald, Quantum gravity and time reversibility, Phys. Rev. D **21**, 2742 (1980).
[7] M. S. Morris and K. S. Thorne, Wormholes in space-time and their use for interstellar travel: A tool for teaching general relativity, Am. J. Phys. **56**, 395 (1988).
[8] Francisco S. N. Lobo, Phantom energy traversable wormholes, Phys. Rev. D **71**, 084011 (2005).
[9] Edward Witten, Light rays, singularities, and all that, Rev. Mod. Phys. **92**, 045004 (2020).
[10] David Hochberg, Lorentzian wormholes in higher order gravity theories, Phys. Lett. B **251**, 349 (1990).
[11] Biplab Bhawal and Sayan Kar, Lorentzian wormholes in Einstein-Gauss-Bonnet theory, Phys. Rev. D **46**, 2464 (1992).
[12] A. G. Agnese and M. La Camera, Wormholes in the Brans-Dicke theory of gravitation, Phys. Rev. D **51**, 2011 (1995).
[13] H. Fukutaka, K. Tanaka, and K. Ghoroku, Wormhole solutions in higher derivative gravity, Phys. Lett. B **222**, 191 (1989).
[14] K. Ghoroku and T. Soma, Lorentzian wormholes in higher derivative gravity and the weak energy condition, Phys. Rev. D **46**, 1507 (1992).
[15] N. Furey and A. DeBenedictis, Wormhole throats in R^m gravity, Classical Quantum Gravity **22**, 313 (2005).
[16] K. A. Bronnikov and E. Elizalde, Spherical systems in models of nonlocally corrected gravity, Phys. Rev. D **81**, 044032 (2010).

[17] Francisco S. N. Lobo, General class of wormhole geometries in conformal Weyl gravity, Classical Quantum Gravity **25**, 175006 (2008).
[18] Panagiota Kanti, Burkhard Kleihaus, and Jutta Kunz, Wormholes in dilatonic Einstein-Gauss-Bonnet theory, Phys. Rev. Lett. **107**, 271101 (2011).
[19] Panagiota Kanti, Burkhard Kleihaus, and Jutta Kunz, Stable Lorentzian wormholes in dilatonic Einstein-Gauss-Bonnet theory, Phys. Rev. D **85**, 044007 (2012).
[20] M. Zubair, Farzana Kousar, and Sebastian Bahamonde, Static spherically symmetric wormholes in generalized $f(R,\phi)$ gravity, Eur. Phys. J. Plus **133**, 523 (2018).
[21] Rajibul Shaikh and Sayan Kar, Wormholes, the weak energy condition, and scalar-tensor gravity, Phys. Rev. D **94**, 024011 (2016).
[22] Ali Övgün, Kimet Jusufi, and İzzet Sakallı, Exact traversable wormhole solution in bumblebee gravity, Phys. Rev. D **99**, 024042 (2019).
[23] Pedro Cañate, Joseph Sultana, and Demosthenes Kazanas, Ellis wormhole without a phantom scalar field, Phys. Rev. D **100**, 064007 (2019).
[24] Ratbay Myrzakulov, Lorenzo Sebastiani, Sunny Vagnozzi, and Sergio Zerbini, Static spherically symmetric solutions in mimetic gravity: Rotation curves and wormholes, Classical Quantum Gravity **33**, 125005 (2016).
[25] De-Chang Dai, Djordje Minic, and Dejan Stojkovic, How to form a wormhole, Eur. Phys. J. C **80**, 1103 (2020).
[26] Mostafizur Rahman, Anjan A. Sen, and Sunil Singh Bohra, Traversable wormholes in bimetric gravity, Phys. Rev. D **108**, 104008 (2023).
[27] Matt Visser, Sayan Kar, and Naresh Dadhich, Traversable wormholes with arbitrarily small energy condition violations, Phys. Rev. Lett. **90**, 201102 (2003).
[28] H. G. Ellis, Ether flow through a drainhole: A particle model in general relativity, J. Math. Phys. (N.Y.) **14**, 104 (1973).
[29] K. A. Bronnikov, Scalar-tensor theory and scalar charge, Acta Phys. Pol. B **4**, 251 (1973), http://inis.iaea.org/search/search.aspx?orig_q=RN:06207385.
[30] Xiao Yan Chew, Burkhard Kleihaus, and Jutta Kunz, Geometry of spinning Ellis wormholes, Phys. Rev. D **94**, 104031 (2016).
[31] Xiao Yan Chew, Burkhard Kleihaus, and Jutta Kunz, Spinning wormholes in scalar-tensor theory, Phys. Rev. D **97**, 064026 (2018).
[32] Xiao Yan Chew and Kok-Geng Lim, Non-Abelian wormholes threaded by a Yang-Mills-Higgs field in the BPS limit, Phys. Rev. D **102**, 124068 (2020).
[33] Jose Luis Blázquez-Salcedo, Xiao Yan Chew, Jutta Kunz, and Dong-Han Yeom, Ellis wormholes in anti–de Sitter space, Eur. Phys. J. C **81**, 858 (2021).
[34] Takashi Torii and Hisa-aki Shinkai, Wormholes in higher dimensional space-time: Exact solutions and their linear stability analysis, Phys. Rev. D **88**, 064027 (2013).
[35] Sayan Kar, Shiraz Minwalla, D. Mishra, and D. Sahdev, Resonances in the transmission of massless scalar waves in a class of wormholes, Phys. Rev. D **51**, 1632 (1995).
[36] Poulami Dutta Roy, S. Aneesh, and Sayan Kar, Revisiting a family of wormholes: Geometry, matter, scalar quasinormal modes and echoes, Eur. Phys. J. C **80**, 850 (2020).
[37] Sunny Vagnozzi *et al.*, Horizon-scale tests of gravity theories and fundamental physics from the Event Horizon Telescope image of Sagittarius A, Classical Quantum Gravity **40**, 165007 (2023).
[38] Sebastian Murk, Nomen non est omen: Why it is too soon to identify ultra-compact objects as black holes, Int. J. Mod. Phys. D **32**, 2342012 (2023).
[39] F. Abe, Gravitational microlensing by the Ellis wormhole, Astrophys. J. **725**, 787 (2010).
[40] Yukiharu Toki, Takao Kitamura, Hideki Asada, and Fumio Abe, Astrometric image centroid displacements due to gravitational microlensing by the Ellis wormhole, Astrophys. J. **740**, 121 (2011).
[41] Ryuichi Takahashi and Hideki Asada, Observational upper bound on the cosmic abundances of negative-mass compact objects and Ellis wormholes from the Sloan digital sky survey quasar lens search, Astrophys. J. Lett. **768**, L16 (2013).
[42] John G. Cramer, Robert L. Forward, Michael S. Morris, Matt Visser, Gregory Benford, and Geoffrey A. Landis, Natural wormholes as gravitational lenses, Phys. Rev. D **51**, 3117 (1995).
[43] Volker Perlick, On the exact gravitational lens equation in spherically symmetric and static space-times, Phys. Rev. D **69**, 064017 (2004).
[44] Naoki Tsukamoto, Tomohiro Harada, and Kohji Yajima, Can we distinguish between black holes and wormholes by their Einstein ring systems?, Phys. Rev. D **86**, 104062 (2012).
[45] Cosimo Bambi, Can the supermassive objects at the centers of galaxies be traversable wormholes? The first test of strong gravity for mm/sub-mm very long baseline interferometry facilities, Phys. Rev. D **87**, 107501 (2013).
[46] C. V. Vishveshwara, Scattering of gravitational radiation by a Schwarzschild black-hole, Nature (London) **227**, 936 (1970).
[47] Caio F. B. Macedo, Vitor Cardoso, Luís C. B. Crispino, and Paolo Pani, Quasinormal modes of relativistic stars and interacting fields, Phys. Rev. D **93**, 064053 (2016).
[48] R. A. Konoplya and A. Zhidenko, Quasinormal modes of black holes: From astrophysics to string theory, Rev. Mod. Phys. **83**, 793 (2011).
[49] Vitor Cardoso, Quasinormal modes and gravitational radiation in black hole spacetimes, Other thesis, Universidade Técnica de Lisboa, Instituto Superior Técnico, 2003.
[50] Kostas D. Kokkotas and Bernd G. Schmidt, Quasinormal modes of stars and black holes, Living Rev. Relativity **2**, 2 (1999).
[51] Paolo Pani, Advanced methods in black-hole perturbation theory, Int. J. Mod. Phys. A **28**, 1340018 (2013).
[52] Kirill A. Bronnikov, Roman A. Konoplya, and Thomas D. Pappas, General parametrization of wormhole spacetimes and its application to shadows and quasinormal modes, Phys. Rev. D **103**, 124062 (2021).
[53] Shauvik Biswas, Mostafizur Rahman, and Sumanta Chakraborty, Echoes from braneworld wormholes, Phys. Rev. D **106**, 124003 (2022).
[54] B. P. Abbott *et al.*, Observation of gravitational waves from a binary black hole merger, Phys. Rev. Lett. **116**, 061102 (2016).

[55] B. P. Abbott *et al.*, GW151226: Observation of gravitational waves from a 22-solar-mass binary black hole coalescence, Phys. Rev. Lett. **116**, 241103 (2016).
[56] Benjamin P. Abbott *et al.*, GW170104: Observation of a 50-solar-mass binary black hole coalescence at redshift 0.2, Phys. Rev. Lett. **118**, 221101 (2017); Phys. Rev. Lett. **121**, 129901(E) (2018).
[57] B. P. Abbott *et al.*, GW170817: Observation of gravitational waves from a binary neutron star inspiral, Phys. Rev. Lett. **119**, 161101 (2017).
[58] Collin D. Capano, Miriam Cabero, Julian Westerweck, Jahed Abedi, Shilpa Kastha, Alexander H. Nitz, Yi-Fan Wang, Alex B. Nielsen, and Badri Krishnan, Observation of a multimode quasi-normal spectrum from a perturbed black hole, Phys. Rev. Lett. **131**, 221402 (2023).
[59] Th. Kaluza, Zum Unitätsproblem der Physik, Sitzungsber. Preuss. Akad. Wiss. Berlin (Math. Phys.) **1921**, 966 (1921).
[60] Oskar Klein, Quantum theory and five-dimensional theory of relativity (in German and English), Z. Phys. **37**, 895 (1926).
[61] Michael B. Green, J. H. Schwarz, and Edward Witten, *Superstring Theory. Vol. 1: Introduction*, Cambridge Monographs on Mathematical Physics (Cambridge University Press, Cambridge, United Kingdom, 2012).
[62] C. Furey, Standard model physics from an algebra?, Ph.D. thesis, Waterloo University, 2015.
[63] John C. Baez, The octonions, Bull. Am. Math. Soc. **39**, 145 (2002); Bull. Am. Math. Soc. **42**, 213(E) (2005).
[64] John C. Baez and John Huerta, Division algebras and supersymmetry II, Adv. Theor. Math. Phys. **15**, 1373 (2011).
[65] N. Furey, Three generations, two unbroken gauge symmetries, and one eight-dimensional algebra, Phys. Lett. B **785**, 84 (2018).
[66] C. Furey, $SU(3)_C \times SU(2)_L \times U(1)_Y (\times U(1)_X)$ as a symmetry of division algebraic ladder operators, Eur. Phys. J. C **78**, 375 (2018).
[67] Adam B. Gillard and Niels G. Gresnigt, Three fermion generations with two unbroken gauge symmetries from the complex sedenions, Eur. Phys. J. C **79**, 446 (2019).
[68] G. R. Dvali, Gregory Gabadadze, and Massimo Porrati, 4-D gravity on a brane in 5-D Minkowski space, Phys. Lett. B **485**, 208 (2000).
[69] V. A. Rubakov and M. E. Shaposhnikov, Do we live inside a domain wall?, Phys. Lett. B **125**, 136 (1983).
[70] Merab Gogberashvili, Our world as an expanding shell, Europhys. Lett. **49**, 396 (2000).
[71] Merab Gogberashvili, Hierarchy problem in the shell universe model, Int. J. Mod. Phys. D **11**, 1635 (2002).
[72] Lisa Randall and Raman Sundrum, A large mass hierarchy from a small extra dimension, Phys. Rev. Lett. **83**, 3370 (1999).
[73] Lisa Randall and Raman Sundrum, An alternative to compactification, Phys. Rev. Lett. **83**, 4690 (1999).
[74] Francisco S. N. Lobo, A general class of braneworld wormholes, Phys. Rev. D **75**, 064027 (2007).
[75] J. Ponce de Leon, Static wormholes on the brane inspired by Kaluza-Klein gravity, J. Cosmol. Astropart. Phys. 11 (2009) 013.
[76] K. C. Wong, T. Harko, and K. S. Cheng, Inflating wormholes in the braneworld models, Classical Quantum Gravity **28**, 145023 (2011).
[77] Sayan Kar, Sayantani Lahiri, and Soumitra SenGupta, Can extra dimensional effects allow wormholes without exotic matter?, Phys. Lett. B **750**, 319 (2015).
[78] Ayan Banerjee, P. H. R. S. Moraes, R. A. C. Correa, and G. Ribeiro, Wormholes in Randall-Sundrum braneworld, arXiv:1904.10310.
[79] Deng Wang and Xin-He Meng, Traversable braneworld wormholes supported by astrophysical observations, Front. Phys. (Beijing) **13**, 139801 (2018).
[80] Sayan Kar, Wormholes with a warped extra dimension?, Gen. Relativ. Gravit. **54**, 66 (2022).
[81] Vivek Sharma and Suman Ghosh, Generalised Ellis–Bronnikov wormholes embedded in warped braneworld background and energy conditions, Eur. Phys. J. C **81**, 1004 (2021).
[82] Vivek Sharma and Suman Ghosh, Geodesics in generalised Ellis–Bronnikov spacetime embedded in warped 5D background, Eur. Phys. J. C **82**, 702 (2022).
[83] Vivek Sharma and Suman Ghosh, Geodesic congruences in 5D warped Ellis–Bronnikov spacetimes, Eur. Phys. J. Plus **137**, 881 (2022).
[84] Vladimir Dzhunushaliev, Vladimir Folomeev, and Masato Minamitsuji, Thick brane solutions, Rep. Prog. Phys. **73**, 066901 (2010).
[85] Ratna Koley and Sayan Kar, Scalar kinks and fermion localisation in warped spacetimes, Classical Quantum Gravity **22**, 753 (2005).
[86] Xin-Hui Zhang, Yu-Xiao Liu, and Yi-Shi Duan, Localization of fermionic fields on braneworlds with bulk tachyon matter, Mod. Phys. Lett. A **23**, 2093 (2008).
[87] Suman Ghosh and Sayan Kar, Bulk spacetimes for cosmological braneworlds with a time-dependent extra dimension, Phys. Rev. D **80**, 064024 (2009).
[88] R. A. Konoplya and A. V. Zhidenko, Decay of massive scalar field in a Schwarzschild background, Phys. Lett. B **609**, 377 (2005).
[89] Alexander Zhidenko, Linear perturbations of black holes: Stability, quasi-normal modes and tails, Ph.D. thesis, São Paulo University, 2009.
[90] Gary T. Horowitz and Veronika E. Hubeny, Quasinormal modes of AdS black holes and the approach to thermal equilibrium, Phys. Rev. D **62**, 024027 (2000).
[91] Bernard F. Schutz and Clifford M. Will, Black hole normal modes: A semianalytic approach, Astrophys. J. Lett. **291**, L33 (1985).
[92] Sai Iyer and Clifford M. Will, Black hole normal modes: A WKB approach. 1. Foundations and application of a higher order WKB analysis of potential barrier scattering, Phys. Rev. D **35**, 3621 (1987).
[93] R. A. Konoplya, Quasinormal behavior of the d-dimensional Schwarzschild black hole and higher order WKB approach, Phys. Rev. D **68**, 024018 (2003).
[94] M. S. Churilova, R. A. Konoplya, and A. Zhidenko, Arbitrarily long-lived quasinormal modes in a wormhole background, Phys. Lett. B **802**, 135207 (2020).

[95] Carsten Gundlach, Richard H. Price, and Jorge Pullin, Late time behavior of stellar collapse and explosions: 1. Linearized perturbations, Phys. Rev. D **49**, 883 (1994).

[96] S. Chandrasekhar and Steven L. Detweiler, The quasinormal modes of the Schwarzschild black hole, Proc. R. Soc. A **344**, 441 (1975).

[97] S. Aneesh, Sukanta Bose, and Sayan Kar, Gravitational waves from quasinormal modes of a class of Lorentzian wormholes, Phys. Rev. D **97**, 124004 (2018).

[98] Akira Ohashi and Masa-aki Sakagami, Massive quasinormal mode, Classical Quantum Gravity **21**, 3973 (2004).